Facility-Measured Sleep Electroencephalographic Microstructures in Long COVID

Haoqi Sun[1], Rammy Dang[1], Peng Li[2], Wenzhong Xiao[2], Jennifer Scott-Sutherland[3], Kenneth C. Sassower[4], M. Brandon Westover[1], Donna Felsenstein[5], Robert J. Thomas[6], Monika Haack[1], Janet M. Mullington[1,*]

[1] Department of Neurology, Beth Israel Deaconess Medical Center, Boston, MA 02215, USA

[2] Center for Engineering in Medicine and Surgery, Massachusetts General Hospital, Boston, MA 02114, USA

[3] Clinical and Translational Research Center, Beth Israel Deaconess Medical Center, Boston, MA 02215, USA

[4] Department of Neurology, Massachusetts General Hospital, Boston, MA 02114, USA

[5] Department of Medicine, Massachusetts General Hospital, Boston, MA 02114, USA

[6] Division of Pulmonary, Critical Care and Sleep Medicine, Department of Medicine, Beth Israel Deaconess Medical Center, Boston, MA 02215, USA

*Corresponding Author:
Janet Mullington, PhD
Professor of Neurology, Harvard Medical School
Department of Neurology, Beth Israel Deaconess Medical Center
DA-779, 330 Brookline Avenue, Boston, MA 02215, USA
Email: jmulling@bidmc.harvard.edu

ABSTRACT

Study Objectives: Sleep electroencephalographic (EEG) microstructures are related to brain functions, providing a window into the unrefreshing, non-restorative sleep and daytime fatigue symptoms in long COVID (LC) and myalgic encephalomyelitis/chronic fatigue syndrome (ME/CFS). We aim to characterize sleep EEG microstructural differences in individuals with LC and age-sex-matched healthy controls (HC), and also ME/CFS, using overnight in-lab facility-measured polysomnography (PSG).

Methods: 28 LC and 28 HC participants came from a single-center research study. 19 ME/CFS participants came from a single clinical center. Sleep EEG was processed to extract spectral band powers, spindles, slow oscillations (SO, 0.5-1Hz), spindle-SO coupling, brain age index (BAI), alpha-delta patterns, and infraslow oscillation relative band power (ISO, 0.005-0.03Hz).

Results: Compared to HC, LC had higher SO power during wake before sleep and REM sleep. In N2 and N3, LC showed a faster within-spindle frequency drop (chirp) and shorter SO peak duration in the frontal region. LC showed widespread, early spindle-SO coupling phase at SO trough for both fast and slow spindles, with early fast spindle-SO coupling associated with worse sleep quality. ME/CFS shared some differences with LC but had higher SO-uncoupled slow spindle densities in frontal and central regions, more alpha-delta patterns in the first half of the night, and widespread elevated ISO power in the slow sigma band (11-13Hz).

Conclusions: These findings suggest that LC and ME/CFS are associated with plausibly pathological sleep EEG microstructure changes, illuminating the pathobiology of post-infectious processes on brain activity.

KEYWORDS

long COVID, sleep, electroencephalography, encephalomyelitis/chronic fatigue syndrome

CLINICAL TRIAL INFORMATION

Trial 1: Sleep and Inflammatory Resolution Pathway, https://clinicaltrials.gov/study/NCT03377543, NCT03377543

Trial 2: Pain in Long COVID-19: the Role of Sleep, https://clinicaltrials.gov/study/NCT05606211, NCT05606211

STATEMENT OF SIGNIFICANCE

People with long COVID (LC) frequently experience sleep disturbances, non-restorative sleep, and fatigue. Sleep electroencephalographic (EEG) microstructures may offer objective markers of subjective sleep quality in LC. Here, we present an in-lab facility-measured sleep study. LC participants exhibited abnormally early spindle-slow oscillation (SO) coupling phase at the trough of the SO, and a faster drop in within-spindle frequency. The abnormally early spindle-SO coupling phase in LC was correlated with worse subjective sleep quality. Similar differences in EEG microstructural patterns were found in people with myalgic encephalomyelitis/chronic fatigue syndrome (ME/CFS) as well. The results demonstrate candidate electrophysiological abnormalities associated with the fatigue and non-restorative sleep experienced in LC.

INTRODUCTION

The post-acute sequelae of SARS-CoV-2 infection, also named long COVID (LC), is defined as an infection-associated chronic condition that occurs after SARS-CoV-2 infection and is present for at least three months as a continuous, relapsing and remitting, or progressive state that affects one or more organ systems[1]. Common symptoms include fatigue, brain fog, and sleep disturbances[2], which significantly impair daily functioning and quality of life. These symptoms closely resemble those of myalgic encephalomyelitis/chronic fatigue syndrome (ME/CFS)[3,4], a disease with persistent fatigue, cognitive dysfunction, and non-refreshing sleep. These symptoms suggest an underlying disruption in brain health, which may involve vascular and neurovascular dysfunction[5,6] or neuroinflammation[7,8]. A major challenge is the lack of objective biomarkers that capture the hallmark symptom of non-restorative sleep despite relatively modest abnormalities in conventional sleep architecture. However, the impact of viral infections and neuro-immunological responses in LC on brain health remains unclear.

Electroencephalographic (EEG) microstructures of sleep are explicitly related to brain and body functions[9,10], providing a unique window into the physiology and pathology of LC, and going beyond the known subjective sleep quality[11] and sleep architectural changes (macrostructure)[12] in LC. Importantly, EEG microstructure metrics may help bridge the long-recognized discrepancy between subjective sleep quality and objective polysomnographic measures such as N3 duration or wake after sleep onset (WASO). For example, delta band power in non-rapid eye movement (NREM) stage 3 (N3) reflects the net effect of circadian and sleep homeostasis[13]; its reduction across the sleep period reflects plasticity homeostasis[14]; spindles and their coupling to slow oscillations (SO, 0.5-1Hz) are related to memory consolidation[10,15]; alpha-delta (alpha intrusion) is associated with chronic fatigue[16]; and infraslow oscillations (ISO) associated with norepinephrine-induced glymphatic clearance[17–21]. Disruptions in sleep EEG microstructures have been linked to brain aging[22], cognitive impairments[23–26], metabolic disorders[27,28], cardiovascular diseases[9], and all-cause mortality[29,30]. Yet, the changes in sleep EEG microstructures in LC are largely unexplored. Identifying such features could provide candidate

physiological markers of non-restorative sleep and potentially enable objective monitoring of disease severity or treatment effects.

Here, we compared the sleep EEG microstructures in individuals with LC to age-sex-matched healthy controls (HCs) using facility-measured, in-lab overnight polysomnography (PSG), which is the gold standard for recording sleep. We aimed to characterize the differences in sleep EEG microstructures between the groups, which may underlie the persistent symptoms of LC.

METHODS

Study Design and Cohort

This was an observational study. Participants were recruited through internet advertisements, physical flyers in the Greater Boston Area, postings on ClinicalTrials.gov (NCT03377543 and NCT05606211), and referrals from clinicians at the Critical Illness and COVID-19 Survivorship Clinic in Beth Israel Deaconess Medical Center (BIDMC). The LC participants were enrolled between November 2022 and November 2023. The eligibility criteria were described in our previous study[6]. Briefly, for the LC group, the inclusion criteria were (1) over 18 years of age, (2) confirmed history of SARS-CoV-2 infection based on SARS-CoV-2 antigen testing, and (3) long COVID consistent with diagnostic code ICD-10 U09.9: Post COVID-19 condition, unspecified. The exclusion criteria for LC were (1) pregnant or lactating, or (2) a history of chronic pain before SARS-CoV-2 infection.

The HCs were a convenience sample of individuals from past studies who enrolled in a study of sleep in healthy people[31], hence having different exclusion criteria than the LC participants. Controls were 1:1 matched by sex and age (±5 years) to the LC participants. The control participants were enrolled between July 2018 and May 2022. The eligibility criteria have been described in our previous publication[6], and can be found in the Supplementary Methods. The HCs did not have any self-reported COVID infection before the initial screening sleep study, although they could be asymptomatic.

The ME/CFS patient cohort was obtained from Massachusetts General Hospital (MGH) in 2022. The inclusion criteria are (1) had an overnight sleep PSG; and (2) had their last ME/CFS diagnosis date in 2022, indicating continuous care for ME/CFS. All eligible PSGs were performed between 2019 and 2022. The data use was approved by the BIDMC Institutional Review Board 2021P001064 under the exempt category 4.

Sleep EEG Microstructures

Eligible participants underwent facility-measured, in-lab overnight polysomnography (PSG). The recordings were conducted using RemLogic or Natus PSG equipment and were scored by one technician following the AASM 2012 scoring manual[32]. There were six EEG channels: F3-M2, F4-M1, C3-M2, C4-M1, O1-M2, and O2-M1. The signals were resampled to 200 Hz. EEG signals were first notch-filtered at 60 Hz and then band-pass filtered from 0.3 to 35 Hz. To remove artifacts, we excluded 30-second epochs containing absolute signal amplitudes higher than 500μV, flat signal (peak-to-peak amplitude < 0.1μV lasting longer than 15 seconds), or having all Hjorth parameters (activity, mobility, complexity) more than 5 standard deviations away from the overnight mean. We then removed electrocardiographic (ECG) artifacts by subtracting the average EEG signature time-aligned to the R peaks, based on a single-channel polarity-corrected ECG signal.

We extracted a comprehensive list of sleep EEG microstructure features. For spectral band powers, we extracted SO (0.5-1Hz), delta (1-4Hz), theta (4-8Hz), alpha (8-12Hz), and beta (12-30Hz) band powers averaged across epochs in N3, N2, N1, REM, wake before sleep onset (WBSO), and WASO, using multi-taper spectral estimation[33,34]. The band powers were converted to decibels, where decibel = $10\times\log_{10}(uV^2)$. The overnight decline of delta band power in N2 and N3 was calculated, which is a measure of sleep homeostasis. There is a normal time-of-night decrement of delta power during sleep, while persistence may signify biological inefficiencies in reducing sleep debt. We also computed alpha-

delta patterns, measured by the average alpha-to-delta ratio across all NREM epochs and those in the first half of the night.

The spindle, SO, and their coupling metrics were derived from N2 or N3 using Luna (version 0.99)[35]. The spindles were detected using wavelet transformation with a cycle number of 7 and a multiplicative threshold of 4.5. To account for the diverse spindle frequencies both across and within individuals, we considered all possible frequencies in the broad sigma range (10.5Hz to 15.5Hz, step size 0.5Hz), and then combined the detection results based on temporal overlap within each channel. For quality control, we first ran the detection with a relaxed quality threshold (q=0 in Luna, definition in the Supplementary Methods), then randomly selected 718 spindles and manually labeled them as spindle or not. We determined the optimal threshold q = 0.62 based on Youden's operating point on the receiver operating characteristic curve (ROC) (Figure S1). The group-wise spindle detection performance and comparisons between groups are shown in Table S1, where there were no significant differences across all groups. We re-ran the detection with the optimal quality threshold. The spindle metrics included (SO-coupled and uncoupled) density, frequency, duration, chirp (the rate of instantaneous frequency change within a spindle, Figure S2), and integrated intensity (a measure of duration and amplitude, normalized by the individual's baseline). The SOs were detected by first band-pass filtering the signal between 0.5-4Hz, finding all zero-crossings, retaining intervals between 0.8-2.0 seconds and negative-peak and peak-to-peak amplitudes, higher than 3 times the median (a relative rule, about 75 μV in middle-aged participants). These steps closely match the definition of slow oscillations, while using the relative rule to become adaptive to the data, such as smaller EEG amplitude associated with older age that artificially reduces the amount of N3. The SO metrics included peak-to-peak amplitude, duration, density, slope, negative slope, and positive slope. The spindle-SO coupling overlap was measured by the proportion of spindles that overlap with SO in the same channel. The spindle-SO coupling phase was calculated by first applying the Hilbert-Huang transformation to obtain the instantaneous phase of the detected SOs, taking the phase at the center of the coupled spindles, and then taking the circular average of the phases across

all coupled spindles. The coupling metrics were calculated for fast spindles (≥13Hz) and slow spindles (<13Hz) separately[35]. 12Hz is also used in the literature[36].

We also calculated the sleep EEG-based brain age index (BAI) as previously described[22] and implemented in Luna[35]. The brain age (BA) is computed as the weighted sum of sleep EEG spectral power and spindle-SO metrics. The brain age index (BAI) was computed as BA minus chronological age. The infraslow oscillation (ISO) power at around 0.02Hz was quantified using the power of sigma power based on an established method[21]. For each brain region (frontal, central, and occipital) and spindle type (slow and fast), we extracted the relative ISO band power between 0.005-0.03Hz.

Subjective Sleep Quality Assessments

For the LC group, we used two subjective sleep quality assessments: Consensus Sleep Diary (CSD) Rest Quality[37] and Patient-Reported Outcomes Measurement Information System Sleep Disturbance (PROMIS-SD)[38]. At home, the CSD was administered every morning over a 2-week period using the Research Electronic Data Capture (REDCap) platform. The CSD included multiple items. Here, we focused on self-reported sleep restoration: "How rested or refreshed did you feel when you woke up for the day?", which has five levels ranging from not at all rested (encoded as 1) to very well rested (encoded as 5). The ratings were averaged across the 2-week monitoring period. Therefore, a higher CSD Rest Quality indicates a better sleep quality. Meanwhile, in the lab, the PROMIS-SD, consisting of a series of questions, was administered in the morning, the raw score was obtained, converted to a T-score, and dichotomized at a score of 60. A T-score ≥ 60 indicated high sleep disturbance (encoded as 1), and a T-score < 60 indicated low sleep disturbance (encoded as 0). Therefore, a higher PROMIS-SD indicates a worse sleep quality.

Statistical Analysis

We used partial Spearman's correlation[39] between the group (HC, LC, ME/CFS) and sleep EEG microstructures (continuous variable) to obtain a covariate-adjusted, rank-based estimate of group differences. This approach assesses monotonic associations that are less dependent on distribution assumptions, such as outliers and skewness in EEG microstructures. In contrast, linear models with small to moderate sample sizes are sensitive to deviations from normality. Conceptually, the partial Spearman approach is analogous to a rank-based ANCOVA. We adjusted for body mass index (BMI) since it may impact sleep. We did not adjust for age and sex since they are matched by design (see Table 1). We did not adjust for AHI, as no participant had a high AHI (>10/hour). Medication and comorbidity were not adjusted due to small sample sizes. As shown in Table S2, the maximum number of participants across medications was 8. In Table S3, we compared sleep patterns between people on medication and those not within the LC group using the Mann-Whitney U test. Similarly, in Table S4, we compared sleep patterns between people with certain pre-COVID comorbidities and those not within the LC group. We used the Bonferroni multiple test correction to control the family-wise error rate, where the number of independent tests was based on principal component analysis (PCA)[40] that explains 99% of the variance in different feature categories separately. The resulting numbers of independent tests were 27 for band powers, 16 for spindle features, 3 for SO features, and 6 for ISO features. The associations between sleep EEG microstructures and subjective sleep quality measures were assessed using partial Spearman's correlation, adjusting for age, sex, and BMI. For this analysis, we did not perform the Bonferroni correction due to its exploratory nature. Statistical analyses were performed using Python 3.10.12.

RESULTS

Cohort Characteristics

The cohort consisted of 28 LC participants and 28 age-sex-matched HC participants. The cohort characteristics are shown in Table 1. Participants were about 37 to 38 years old on average, with 71.4% being female. By design, there were no significant differences in age and sex. There were no Asian or Black participants in the LC group, in contrast to the HC. The median time since the COVID-19 infection index date was 1.3 years. The LC group had reduced total sleep time, about 8% lower sleep efficiency, about three times longer sleep latency, spent less time in REM sleep, mainly during the second half of the night, and had approximately twice the REM latency than HC. The lower REM duration in LC is not a byproduct of reduced total sleep time, since the REM percent is also lower. In the LC group, the subjective sleep quality measure, CSD Rest Quality (1 is worst resting, 5 is best resting), has a median of 2.4, while PROMIS-SD (binary) indicates 8 (28.6%) participants experienced high sleep disturbance. The medications, comorbidities before COVID-19 infection, and LC symptoms of the LC group are described in Table S2. In Figure S5, we show example EEG spectrograms and hypnograms from the HC, LC, and ME/CFS groups.

We did not find significant differences between HC and LC in alpha-delta patterns ($p = 0.58$), brain age index (BAI, +0.4 years in HC and +1.0 years in LC, $p = 0.39$), or overnight delta power reduction ($p = 0.54$). The following subsections describe the positive findings. The HC vs. LC results are shown in Table 2.

Band Power Comparison Results

The band power comparison results are in Table 2. Compared to HC, SO power (0.5-1Hz) was higher in LC during REM and wake before sleep onset (WBSO) ($p<0.001$). These differences in the frontal region are illustrated in Figure 1. The LC group also had higher delta power (1-4Hz) at WBSO and N1 in the

frontal region, and higher beta power (12-30Hz) at WBSO, both of which did not survive the Bonferroni correction. The spectra in the central and occipital regions are presented in Figures S3 and S4, respectively.

Spindle Comparison Results

The spindle comparison results are in Table 2. There was no difference in the spindle density, amplitude, frequency, or duration between HC and LC. The fast spindle chirp at the central channels exhibited a quicker drop in the within-spindle frequency, as measured by a more negative chirp in the LC group at a median of -0.32Hz/s, where the HC group had -0.20Hz/s ($p < 0.001$). The correlations between fast spindle chirp and SO phase in the central and frontal regions were weaker in the LC group (0.27-0.36) compared to the HC group (0.45-0.51) ($p < 0.01$), representing a more variable SO-phase modulation of within-spindle frequency.

In Figure 2, we show the more detailed instantaneous frequency (IF) within spindles, stratified by channel and spindle type (slow and fast). The slow spindles (<13Hz) showed a U-shape IF, while the fast spindles (≥13Hz) showed an inverted U-shape IF. For fast spindles at the central channels, the frequency difference occurs in the second half of the spindle, leading to a more negative spindle chirp.

Slow Oscillation Comparison Results

The SO comparison results are in Table 2. The duration of the SO positive peak was shorter in LC at 0.45 seconds compared to HC at 0.50 seconds ($p < 0.001$). Meanwhile, the SO rising slope was steeper in the LC at 326.3uV/s than in the HC at 264.3uV/s ($p < 0.01$).

Spindle-Slow Oscillation Coupling Comparison Results

Figure 3 shows the spectrograms time-aligned to the SO negative peaks. In HC (Figure 3A), the spindles were coupled around the SO positive peak. While in LC (Figure 3B), the spindle-SO coupling phase was advanced as early as the SO negative peak, which is an abnormal and widespread phenomenon. The widespread phase advance in LC was present in both fast and slow spindles, which was most evident in fast spindles due to their later coupling phase in HC. The results were consistent with those in the coupling phase, as shown in Table 2.

Infraslow Oscillation Comparison Results

The ISO comparison results are in Table 2. The LC group had a higher ISO relative band power (0.005-0.03Hz) at slow spindle (11-13Hz) at the frontal region, where the control group had a median of 35% and the LC group at 38% ($p < 0.01$). There was no difference in other spindle types or brain regions. Figure S9 shows the detailed ISO power spectral density (PSD), where the ISO PSD of slow spindles at the frontal region of the LC group had higher power than the HC, consistent with the results in Table 2. In both groups, the ISO peak frequency was slowest in the occipital region, followed by the central region, and the frontal region.

Clinical ME/CFS Cohort Comparison Results

Table 1 also describes the characteristics of the clinical ME/CFS cohort and their sleep architectures. The ME/CFS participants were about 41 years old on average, and 74% were female. There were no significant differences in age and sex compared to HC. There were no Asian or Black participants in the ME/CFS group. Compared to HC, the ME/CFS group had about 5% lower sleep efficiency, about three times longer sleep latency, less time spent in REM regardless of the first or second half of the night, about

twice the REM latency, and more continuous N1. The complete HC vs. ME/CFS EEG microstructure comparison results are in Table 2.

Compared to HC, during N3, the ME/CFS group had higher power in the beta band in the occipital region. Figure 4A, Figure S6, and Figure S7 show the detailed spectra comparison with additional differences, which became insignificant after Bonferroni correction. When comparing the alpha-delta patterns to HC, the ME/CFS group showed an initially higher alpha-to-delta ratio in the occipital region in the first half of NREM sleep ($p=0.005$), which became insignificant after Bonferroni correction. Similarly, for overnight delta power reduction, the ME/CFS showed an initially less negative reduction in the central region ($p=0.036$), which became insignificant after Bonferroni correction. Additionally, we did not find significant differences in BAI (+0.4 years in HC and -0.3 years in ME/CFS, $p = 0.53$).

When comparing the spindle and SO patterns to HC, similar to LC, the widespread phase advance in ME/CFS was present in both fast and slow spindles, with the most pronounced effect observed in fast spindles (Figure S8). For the slow spindles, there was an increased slow spindle density in the central region. However, a further decomposition into SO-coupled and SO-uncoupled spindles showed that the increased density was only in SO-uncoupled slow spindles. For the fast spindles, the ME/CFS group also had a more negative fast spindle chirp compared to the controls (Figure 4B), a pattern similar to that seen in the LC group. However, there was no significant difference in SO-phase correlation with the within-spindle frequency compared to HC. There were also no differences in SO characteristics compared to HC.

Compared to HC, the ME/CFS group had a higher ISO relative band power across all regions using the slow sigma band and a higher ISO relative band power in the occipital region using the fast sigma band. As shown in Figure 4C, the ISO PSDs exhibit a higher and more concentrated peak at around 0.02Hz.

When comparing ME/CFS and LC, we did not find differences for the features in Table 2. On the other hand, differences were found in other features: ME/CFS patients had a lower frontal delta power at wake before sleep onset than LC patients (ME/CFS median 15.5dB, LC median 20.5dB, $p < 0.001$); ME/CFS patients also had a higher alpha-to-delta ratio in the occipital region in the first half of NREM sleep than

LC patients (ME/CFS median 0.35, LC median 0.21, p = 0.009) that similarly became insignificant after Bonferroni correction.

Association Results with Subjective Sleep Quality

As shown in Table 3, the sleep EEG microstructures with positive correlation with the Consensus Sleep Diary (CSD) rest quality (the higher the better, $p<0.05$) included fast spindle-SO coupling phase at the central region, fast spindle-SO coupling overlap at the occipital region, and SO density at the occipital region. The sleep EEG microstructures with negative correlation with the CSD rest quality (the lower the better, $p<0.05$) included frontal theta power (4-8Hz) at N2 or N3, the min-max range of fast spindle frequency at central and occipital regions, coupled fast spindle density and fast spindle frequency in the occipital region. Additionally, the N2 continuation probability had a positive Spearman's correlation with CSD rest quality (0.54 [0.19, 0.77], $p < 0.01$).

As shown in Table 3, the sleep EEG microstructures with positive correlation with the Patient-Reported Outcomes Measurement Information System Sleep Disturbance (PROMIS-SD, the higher the worse, $p<0.05$) included min-max range of slow spindle frequency, SO phase correlation with the slow spindle frequency, and SO positive slope at the central region. There was no common microstructure associated with the CSD rest quality. On the other hand, the SO density in the occipital region was negatively associated with PROMIS-SD, which was also associated with CSD rest quality in the opposite and expected direction. Additionally, the N1 continuation probability had a negative Spearman's correlation with PROMIS-SD (-0.45 [-0.71, -0.08], $p<0.05$).

DISCUSSION

In this observational study, we compared the sleep EEG microstructures between participants with long COVID and healthy controls using overnight sleep studies conducted in an in-lab facility.

One key finding is that spindle morphology differed between groups, despite density, amplitude, duration, and frequency being similar. The spindle morphological differences include a more negative spindle chirp (rate of IF change), a weaker correlation between IF and SO phase, and an advanced SO-coupling phase in LC. Spindles are generated in the thalamus, propagated to the cortex, and form a feedback loop between the cortex and thalamus[10]. Although the impairment mechanism is unknown in LC, the thalamocortical feedback loop is possibly impaired by a few mechanisms, e.g., 1) an excitation/inhibition imbalance from a glial pro-inflammatory responses[41–43] to viral infection; 2) mitochondrial impairment[44] 3) redox-stress from a lower nocturnal SpO_2[6], all contributing to impaired synchronization of spike timing at the dendritic level[45]. Therefore, there could be an insufficient "push" for spindle activity, as reflected in an abnormal coupling phase. The weaker correlation between the IF and SO phases may suggest that the cortex-to-thalamus circuit is involved in the abnormality, as the SO is a cortical phenomenon that modulates spindling activity. Meanwhile, reduced precision of the spindle-SO coupling phase is associated with amyloid positivity and higher Aβ42/Aβ40 in cerebrospinal fluid[46], suggesting that LC may share common pathophysiology with Alzheimer's disease, such as neuroinflammation and blood-brain barrier disruption[47–50]. A possible consequence of impaired spindle-SO coupling in LC could be impaired sleep-dependent memory consolidation[15], which is age-dependent[51]. A similarly altered spindle chirp can be found in autism spectrum disorder (ASD)[52], with abnormal EEG functional connectivity at high frequencies[53,54]. Similarly, ASD is associated with mitochondrial impairment[55] and neuroinflammation[56]. Interestingly, spindle characteristics in ME/CFS and LC share differences in terms of spindle chirp and advanced spindle-SO coupling phase, while also showing distinct differences in increased SO-uncoupled slow spindle density in frontal and central regions (Table 2), compared with HC. Many studies have suggested that fast spindles are mainly associated with cognitive performance[36,57]. Therefore, ME/CFS patients may have reduced efficiency in producing fast spindles that support brain health compared to LC patients. The higher SO-uncoupled spindle density in ME/CFS may indicate impaired thalamocortical coordination, which is regulated by arousal centers in the brainstem and

manifests as changes in cyclic alternating pattern (CAP) in ME/CFS patients[58] but not yet studied in LC patients.

For the spectral differences, LC has higher SO power in REM and wake before sleep onset. We can exclude the possibility of an eye movement effect, as the differences did not exhibit a frontal-central-occipital gradient and were consistent across these regions (Figures 1, S3, S4). EEG slowing during REM is associated with cholinergic network dysfunction[59] and mild cognitive impairment[25], which could contribute to the about double REM latency in LC (Table 1). However, our results showed that the REM latency is also longer in ME/CFS, while there is no statistically significant REM slowing in ME/CFS. We further tested the association between SSRI/SNRI antidepressant medication use and REM latency, and found no association ($p>0.05$). Notably, the alpha-delta pattern (alpha intrusion) was not different in LC but was higher in the ME/CFS group before the Bonferroni correction. The alpha-delta pattern is well known for its correlation with fatigue, non-refreshing sleep, and fibromyalgia. However, the neural basis of the alpha-delta pattern remains poorly understood. A computational model generated an alpha-delta pattern by introducing high-threshold thalamocortical (HTC) cells into a thalamic model[60]. Whether ME/CFS patients have more HTC cells than LC patients requires testing.

The ISO relative power was higher in LC participants at the frontal regions from the slow spindle band. ISO has been found to correlate with the rhythmic release of norepinephrine from the locus coeruleus, which enables glymphatic clearance and boosts the flow of blood and cerebrospinal fluid[17]. Our previous work, comparing blood oxygen levels (SpO_2) in the same cohort, showed lower baseline SpO2 in LC participants[6]. Therefore, one hypothesis is that the increase in ISO may reflect a compensatory mechanism to maintain the required total oxygen by increasing blood volume, because of reduced blood oxygen saturation.

No difference was found in the sleep EEG-based brain age index (BAI)[22]. BAI is driven by a selected set of age-dependent sleep EEG features, including delta power, delta-to-alpha ratio, delta-to-theta ratios, spindle density, spindle-SO coupling overlap, and power and waveform kurtosis (measures bursts) in N2

and N3, and alpha power in N1. These patterns were not different between HC and LC, suggesting that LC may represent differences in specific neural dynamics that are insensitive to age. In a broader sense, biological aging is influenced by cumulative stressors such as inflammation, vascular dysfunction, and metabolic stress, many of which have been proposed to be involved in LC, but may not be directly predictive of age.

The associations between sleep EEG microstructures and the subjective sleep quality measures provide new insights. The fast spindle-SO coupling phase, being significantly phase-advanced in LC, is positively correlated with higher diary-based rest quality in LC. Therefore, the fast spindle-SO coupling phase may serve as a marker of the severity of LC-related sleep quality and fatigue. This relationship suggests that EEG microstructure features may serve as candidate biomarkers linking sleep physiology with patient-reported symptoms. Meanwhile, the SO density (number of SO events per minute) correlated with better sleep quality in both subjective and objective measures. SO occurs in N2 and N3 and is the strongest in N3 (conventional slow wave sleep), which is considered the most restorative phase of sleep.

A key question is whether the findings of this study help better understand the spectrum of sleep disorders in LC, which may also point to treatment approaches. Clinical insomnia is common in LC, though cases referred to dedicated sleep-LC programs, such as those that exist in our center, show a spectrum from insomnia, sleep-wake cycle instability, hypersomnia, and even REM-behavior disorder[61]. Low-dose cyclobenzaprine has been used with some success in improving pain and fatigue in fibromyalgia[62,63], a disease with overlapping symptoms with LC and ME/CFS. Sleep spindles are reported as reduced in fibromyalgia[64]. Oxybate (sodium, low sodium) improved hypersomnia symptoms (brain fog, fatigue, sleep quality) in LC[61]. It is plausible that effective treatments normalize the coupling of brain oscillations during sleep, thereby enabling normal sleep functions, with resultant improvements in perceived sleep quality and daytime fatigue symptoms. If validated longitudinally, these EEG microstructure metrics could also provide objective markers for tracking disease progression and response to therapeutic interventions.

Our study has several limitations. First, the sample size was modest. The control group was drawn from historical cohorts and had stricter exclusion criteria than the LC group. Second, some LC participants were taking medications, such as antidepressants and hypnotics (Table S2). As shown in Table S3, within the LC group, pain medication is associated with a more negative spindle chirp, which could explain the more negative spindle chirp in the LC group than in the HC group in Table 2. Similarly, some LC participants had pre-COVID comorbidities, such as sleep apnea, insomnia, depression or anxiety, and headache or migraine (Table S2). However, we did not find common sleep patterns in Table S4 compared with those in Table 2, indicating the results are less affected by pre-COVID comorbidities. In general, a larger sample size is required to adequately account for medications and comorbidities. Third, although in-lab facility-measured polysomnography is the gold standard for recording sleep, a first-night effect can occur, particularly in terms of total sleep time, which may not accurately reflect habitual sleep patterns.

ACKNOWLEDGMENTS

Work was supported by the Open Medicine Foundation and Patient-Led Collaborative (to JMM and WX) and the NHLBI/NINDS/NIAID RECOVER Initiative research studies at Beth Israel Deaconess Medical Center (JMM). Additional research support was provided by the NIH (NIH/NHLBI R01HL136310 and NIH/NINDS R21NS128815, to MH). In addition, we gratefully acknowledge the Harvard Catalyst of the Clinical Research Center through NCATs (NIH/UL1 RR02758 and M01-RR-01032).

DISCLOSURE STATEMENT

Financial Disclosure: MBW is a co-founder, serves as a scientific advisor and consultant to, and has a personal equity interest in Beacon Biosignals.

Non-financial Disclosure: RJT discloses: 1) patent and license/royalties from MyCardio, LLC, for the ECG-spectrogram; 2) patent and license/royalties from DeVilbiss-Drive for an auto-CPAP algorithm; 3) consulting for Jazz Pharmaceuticals, Guidepoint Global and GLG Councils.

Other authors declare that they have no conflict of interest.

DATA AND CODE AVAILABILITY

The dataset and code are available upon reasonable request from the corresponding author(s).

REFERENCES

1. National Academies of Sciences Engineering, Medicine. *A Long COVID Definition: A Chronic, Systemic Disease State with Profound Consequences*. (Fineberg HV, Brown L, Worku T, Goldowitz I, eds.). The National Academies Press; 2024. doi:10.17226/27768
2. Thaweethai T, Jolley SE, Karlson EW, et al. Development of a definition of postacute sequelae of SARS-CoV-2 infection. *Jama*. 2023;329(22):1934-1946.
3. Wong TL, Weitzer DJ. Long COVID and myalgic encephalomyelitis/chronic fatigue syndrome (ME/CFS)—a systemic review and comparison of clinical presentation and symptomatology. *Medicina*. 2021;57(5):418.
4. Komaroff AL, Lipkin WI. ME/CFS and Long COVID share similar symptoms and biological abnormalities: road map to the literature. *Frontiers in Medicine*. 2023;10:1187163.
5. Kempuraj D, Aenlle KK, Cohen J, et al. COVID-19 and long COVID: disruption of the neurovascular unit, blood-brain barrier, and tight junctions. *The Neuroscientist*. 2024;30(4):421-439.
6. Sun H, Dang R, Haack M, et al. Facility-Measured Nocturnal Hypoxemia and Sleep Among Adults with Long COVID versus Age-and Sex-Matched Healthy Adults: A Preliminary Observational Study. *Sleep Advances*. Published online 2025:zpaf017.
7. Kavanagh E. Long Covid brain fog: a neuroinflammation phenomenon? *Oxford open immunology*. 2022;3(1):iqac007.
8. Tate W, Walker M, Sweetman E, et al. Molecular mechanisms of neuroinflammation in ME/CFS and long COVID to sustain disease and promote relapses. *Frontiers in Neurology*. 2022;13:877772.
9. Sun H, Adra N, Ayub MA, et al. Assessing risk of health outcomes from brain activity in sleep: a retrospective cohort study. *Neurology: Clinical Practice*. 2024;14(1):e200225.

10. Fernandez LM, Lüthi A. Sleep spindles: mechanisms and functions. *Physiological reviews*. 2020;100(2):805-868.

11. Batool-Anwar S, Fashanu OS, Quan SF. Long-Term Effects of COVID-19 on Sleep Patterns. *Thoracic Research and Practice*. 2025;26(1):9.

12. Mekhael M, Lim CH, El Hajjar AH, et al. Studying the effect of long COVID-19 infection on sleep quality using wearable health devices: observational study. *Journal of Medical Internet Research*. 2022;24(7):e38000.

13. Borbély AA, others. A two process model of sleep regulation. *Hum neurobiol*. 1982;1(3):195-204.

14. Tononi G, Cirelli C. Sleep and synaptic homeostasis: a hypothesis. *Brain research bulletin*. 2003;62(2):143-150.

15. Klinzing JG, Niethard N, Born J. Mechanisms of systems memory consolidation during sleep. *Nature neuroscience*. 2019;22(10):1598-1610.

16. Van Hoof E, De Becker P, De Meirleir K, Cluydts R, Lapp C. Defining the occurrence and influence of alpha-delta sleep in chronic fatigue syndrome. *The American journal of the medical sciences*. 2007;333(2):78-84.

17. Hauglund NL, Andersen M, Tokarska K, et al. Norepinephrine-mediated slow vasomotion drives glymphatic clearance during sleep. *Cell*. 2025;188(3):606-622.

18. Osorio-Forero A, Foustoukos G, Cardis R, et al. Infraslow noradrenergic locus coeruleus activity fluctuations are gatekeepers of the NREM–REM sleep cycle. *Nature neuroscience*. 2025;28(1):84-96.

19. Fultz NE, Bonmassar G, Setsompop K, et al. Coupled electrophysiological, hemodynamic, and cerebrospinal fluid oscillations in human sleep. *Science*. 2019;366(6465):628-631.

20. Xie L, Kang H, Xu Q, et al. Sleep drives metabolite clearance from the adult brain. *science*. 2013;342(6156):373-377.

21. Lázár ZI, Dijk DJ, Lázár AS. Infraslow oscillations in human sleep spindle activity. *Journal of neuroscience methods*. 2019;316:22-34.

22. Sun H, Paixao L, Oliva JT, et al. Brain age from the electroencephalogram of sleep. *Neurobiology of aging*. 2019;74:112-120.

23. Ye EM, Sun H, Krishnamurthy PV, et al. Dementia detection from brain activity during sleep. *Sleep*. 2023;46(3):zsac286.

24. Adra N, Dümmer LW, Paixao L, et al. Decoding information about cognitive health from the brainwaves of sleep. *Scientific Reports*. 2023;13(1):11448.

25. Lam AKF, Carrick J, Kao CH, et al. Electroencephalographic slowing during REM sleep in older adults with subjective cognitive impairment and mild cognitive impairment. *Sleep*. 2024;47(6).

26. Geng D, Wang C, Fu Z, Zhang Y, Yang K, An H. Sleep EEG-based approach to detect mild cognitive impairment. *Frontiers in aging neuroscience*. 2022;14:865558.

27. Vallat R, Shah VD, Walker MP. Coordinated human sleeping brainwaves map peripheral body glucose homeostasis. *Cell Reports Medicine*. 2023;4(7).

28. Feeney SP, McCarthy JM, Petruconis CR, Tudor JC. Sleep loss is a metabolic disorder. *Science Signaling*. 2025;18(881):eadp9358.

29. Paixao L, Sikka P, Sun H, et al. Excess brain age in the sleep electroencephalogram predicts reduced life expectancy. *Neurobiology of aging*. 2020;88:150-155.

30. Kristjánsson TÓ, Stone KL, Sorensen HB, Brink-Kjaer A, Mignot E, Jennum P. Mortality risk assessment using deep learning-based frequency analysis of electroencephalography and electrooculography in sleep. *Sleep*. 2025;48(2):zsae219.

31. Engert LC, Ledderose C, Biniamin C, et al. Effects of low-dose acetylsalicylic acid on the inflammatory response to experimental sleep restriction in healthy humans. *Brain, Behavior, and Immunity*. 2024;121:142-154.

32. Berry RB. The AASM manual for the scoring of sleep and associated events: rules, terminology and technical specifications. version 2.1. *Darien Illinois: American Academy of Sleep Medicine*. Published online 2014.

33. Thomson DJ. Spectrum estimation and harmonic analysis. *Proceedings of the IEEE*. 2005;70(9):1055-1096.

34. Prerau MJ, Brown RE, Bianchi MT, Ellenbogen JM, Purdon PL. Sleep neurophysiological dynamics through the lens of multitaper spectral analysis. *Physiology*. 2017;32(1):60-92.

35. Purcell S, Manoach D, Demanuele C, et al. Characterizing sleep spindles in 11,630 individuals from the National Sleep Research Resource. *Nature communications*. 2017;8(1):15930.

36. Mölle M, Bergmann TO, Marshall L, Born J. Fast and slow spindles during the sleep slow oscillation: disparate coalescence and engagement in memory processing. *Sleep*. 2011;34(10):1411-1421.

37. Carney CE, Buysse DJ, Ancoli-Israel S, et al. The consensus sleep diary: standardizing prospective sleep self-monitoring. *Sleep*. 2012;35(2):287-302.

38. Buysse DJ, Yu L, Moul DE, et al. Development and validation of patient-reported outcome measures for sleep disturbance and sleep-related impairments. *Sleep*. 2010;33(6):781-792.

39. Kim S. ppcor: An R Package for a Fast Calculation to Semi-partial Correlation Coefficients. *CSAM*. 2015;22(6):665-674. doi:10.5351/CSAM.2015.22.6.665

40. Nicodemus KK, Liu W, Chase GA, Tsai YY, Fallin MD. Comparison of type I error for multiple test corrections in large single-nucleotide polymorphism studies using principal components versus haplotype blocking algorithms. In: *BMC Genetics*. Vol 6. Springer; 2005:1-4.

41. Garcia-Oscos F, Salgado H, Hall S, et al. The stress-induced cytokine interleukin-6 decreases the inhibition/excitation ratio in the rat temporal cortex via trans-signaling. *Biological psychiatry*. 2012;71(7):574-582.

42. Kim K, Abramishvili D, Du S, et al. Meningeal lymphatics-microglia axis regulates synaptic physiology. *Cell*. Published online 2025.

43. Nicolas CS, Peineau S, Amici M, et al. The Jak/STAT pathway is involved in synaptic plasticity. *Neuron*. 2012;73(2):374-390.

44. Molnar T, Lehoczki A, Fekete M, et al. Mitochondrial dysfunction in long COVID: mechanisms, consequences, and potential therapeutic approaches. *Geroscience*. 2024;46(5):5267-5286.

45. Seibt J, Richard CJ, Sigl-Glöckner J, et al. Cortical dendritic activity correlates with spindle-rich oscillations during sleep in rodents. *Nature communications*. 2017;8(1):684.

46. Pulver RL, Kronberg E, Medenblik LM, et al. Mapping sleep's oscillatory events as a biomarker of Alzheimer's disease. *Alzheimer's & Dementia*. 2024;20(1):301-315. doi:10.1002/alz.13420

47. Talkington GM, Kolluru P, Gressett TE, et al. Neurological sequelae of long COVID: a comprehensive review of diagnostic imaging, underlying mechanisms, and potential therapeutics. *Front Neurol*. 2025;15:1465787. doi:10.3389/fneur.2024.1465787

48. Popa E, Popa AE, Poroch M, et al. The Molecular Mechanisms of Cognitive Dysfunction in Long COVID: A Narrative Review. *IJMS*. 2025;26(11):5102. doi:10.3390/ijms26115102

49. Sweeney MD, Sagare AP, Zlokovic BV. Blood–brain barrier breakdown in Alzheimer disease and other neurodegenerative disorders. *Nat Rev Neurol*. 2018;14(3):133-150. doi:10.1038/nrneurol.2017.188

50. Heneka MT, Van Der Flier WM, Jessen F, et al. Neuroinflammation in Alzheimer disease. *Nat Rev Immunol*. 2025;25(5):321-352. doi:10.1038/s41577-024-01104-7

51. Muehlroth BE, Sander MC, Fandakova Y, et al. Precise slow oscillation–spindle coupling promotes memory consolidation in younger and older adults. *Scientific reports*. 2019;9(1):1940.

52. Cumming D, Kozhemiako N, Thurm AE, Farmer CA, Purcell S, Buckley AW. Spindle chirp and other sleep oscillatory features in young children with autism. *Sleep Medicine*. 2024;119:320-328.

53. Bogéa Ribeiro L, da Silva Filho M. Systematic review on EEG analysis to diagnose and treat autism by evaluating functional connectivity and spectral power. *Neuropsychiatric Disease and Treatment*. Published online 2023:415-424.

54. Ke SY, Wu H, Sun H, et al. Classification of autism spectrum disorder using electroencephalography in Chinese children: a cross-sectional retrospective study. *Frontiers in Neuroscience*. 2024;18:1330556.

55. Khaliulin I, Hamoudi W, Amal H. The multifaceted role of mitochondria in autism spectrum disorder. *Molecular psychiatry*. 2025;30(2):629-650.

56. Hughes H, Moreno R, Ashwood P. Innate immune dysfunction and neuroinflammation in autism spectrum disorder (ASD). *Brain, behavior, and immunity*. 2023;108:245-254.

57. Adra N, Sun H, Ganglberger W, et al. Optimal spindle detection parameters for predicting cognitive performance. *Sleep*. 2022;45(4):zsac001.

58. Guilleminault C, Poyares D, Rosa AD, Kirisoglu C, Almeida T, Lopes MC. Chronic fatigue, unrefreshing sleep and nocturnal polysomnography. *Sleep Medicine*. 2006;7(6):513-520. doi:10.1016/j.sleep.2006.03.016

59. Anderson J, Churchill L, Konuri A, et al. Electroencephalographic slowing during REM sleep is a marker of cholinergic dysfunction in Lewy body disorders. *In Review*. Preprint posted online December 2, 2025. doi:10.21203/rs.3.rs-8131680/v1

60. Vijayan S, Klerman EB, Adler GK, Kopell NJ. Thalamic mechanisms underlying alpha-delta sleep with implications for fibromyalgia. *Journal of neurophysiology*. 2015;114(3):1923-1930.

61. Coelho FM, Czuma R, Ticotsky A, Maley J, Mullington JM, Thomas RJ. Sleep disorder syndromes of post-acute sequelae of SARS-CoV-2 (PASC)/Long Covid. *Sleep Medicine*. 2024;123:37-41.

62. Moldofsky H, Harris HW, Archambault WT, Kwong T, Lederman S. Effects of bedtime very low dose cyclobenzaprine on symptoms and sleep physiology in patients with fibromyalgia syndrome: a double-blind randomized placebo-controlled study. *The Journal of rheumatology*. 2011;38(12):2653-2663.

63. Lederman S, Arnold LM, Vaughn B, Kelley M, Sullivan GM. Efficacy and Safety of Sublingual Cyclobenzaprine for the Treatment of Fibromyalgia: Results From a Randomized, Double-Blind, Placebo-Controlled Trial. *Arthritis Care & Research*. 2023;75(11):2359-2368.

64. Landis CA, Lentz MJ, Rothermel J, Buchwald D, Shaver JL. Decreased sleep spindles and spindle activity in midlife women with fibromyalgia and pain. *Sleep*. 2004;27(4):741-750.

FIGURE CAPTIONS

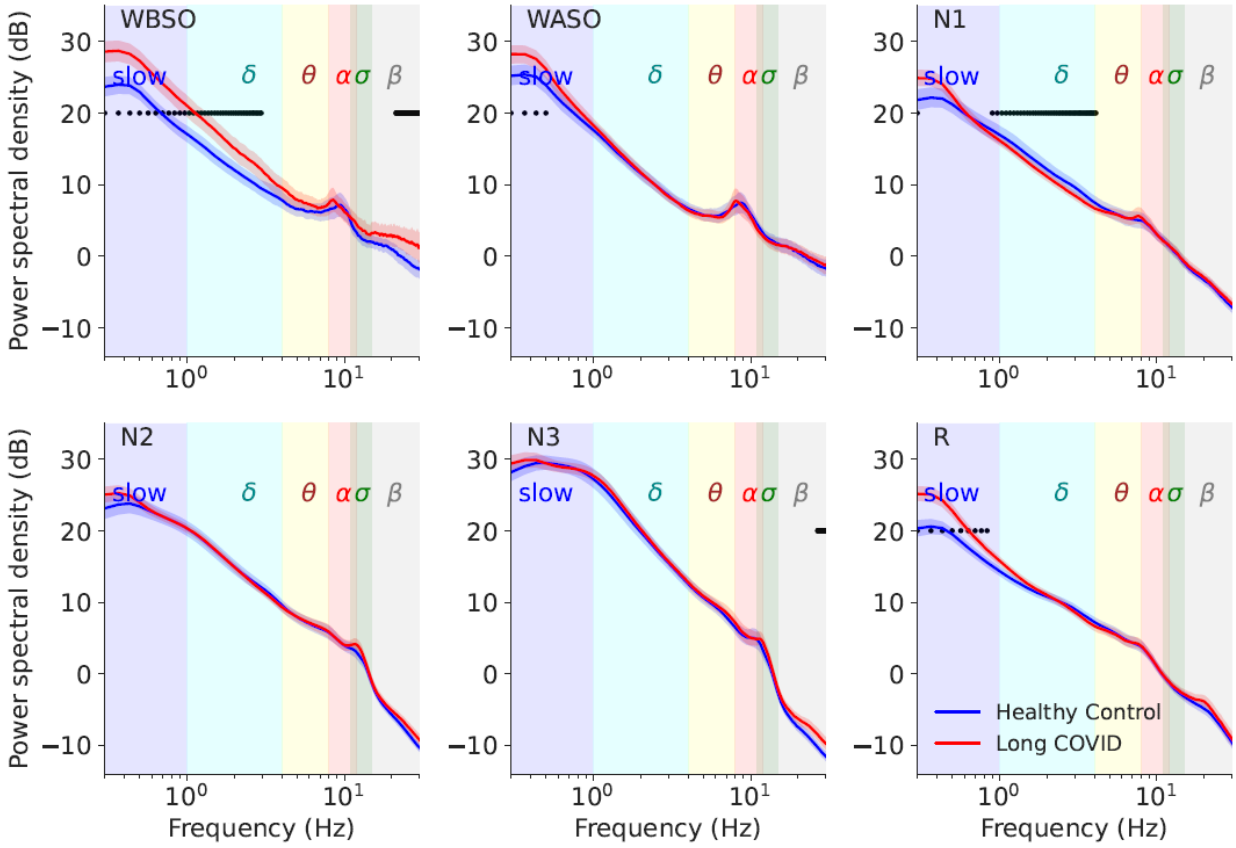

Figure 1. The spectra of different sleep periods and stages for the HC and LC groups, averaged between F3-M2 and F4-M1 channels. The red line represents the LC group. The blue line represents the control group. The power spectral density was calculated over 30-second epochs, converted into decibels (dB = $10\times\log_{10}(uV^2/Hz)$), and averaged over artifact-free epochs in the specified period. The shading represents 95% confidence intervals from bootstrapping 1,000 times. The horizontal solid lines at 20Hz indicate frequencies with significant differences between the two groups. WBSO – wake before sleep onset; WASO – wake after sleep onset.

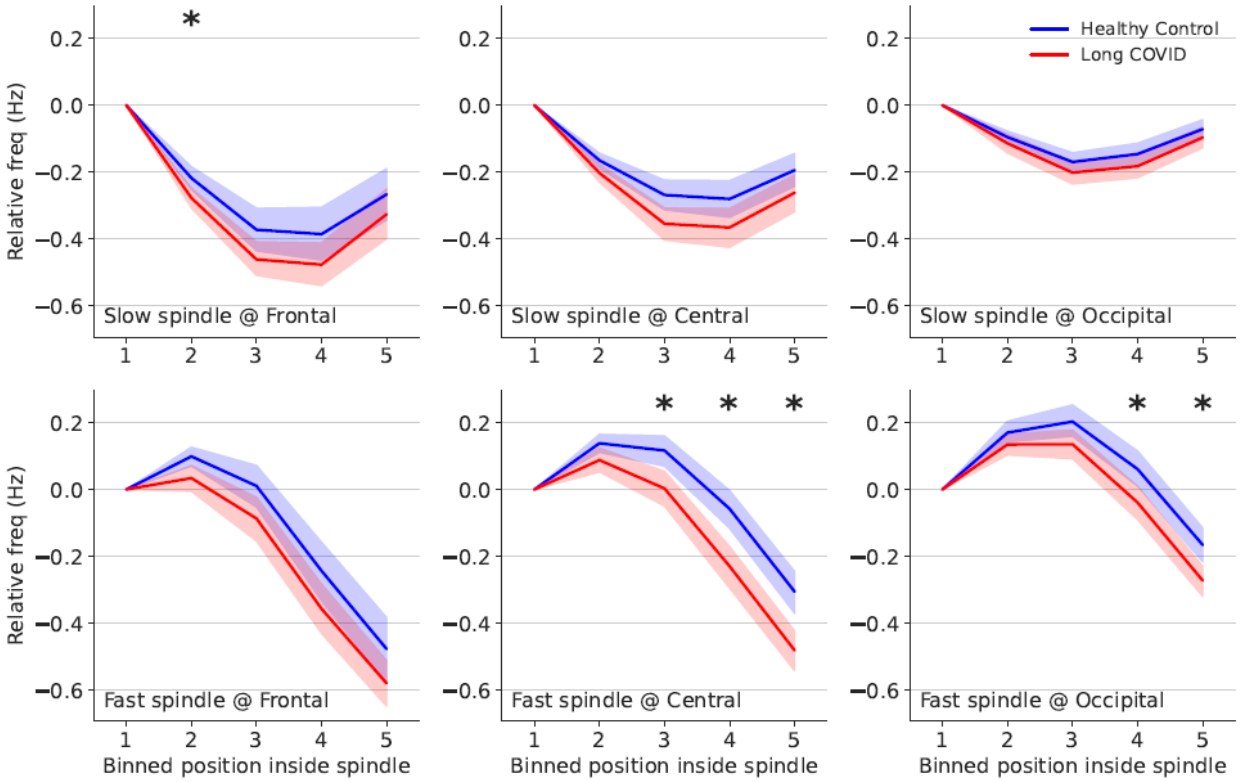

Figure 2. The instantaneous frequency (IF, frequency within a spindle) over the time course within spindles, partitioned into five bins of equal duration for the HC and LC groups. The frequencies are relative to the frequency at the first bin to better show the relative change in frequency over time. The red line represents the LC group. The blue line represents the control group. The shading represents 95% confidence intervals from bootstrapping 1,000 times. The asterisks represent nonoverlapping confidence intervals (i.e., $p<0.05$). The top row shows the slow spindles (<13Hz). The bottom row shows the fast spindles (≥13Hz). The left, center, and right columns represent the frontal, central, and occipital channels, respectively. The instantaneous frequencies at the latter part of the fast spindles at the central and occipital channels were significantly lower in the LC group than in the control group.

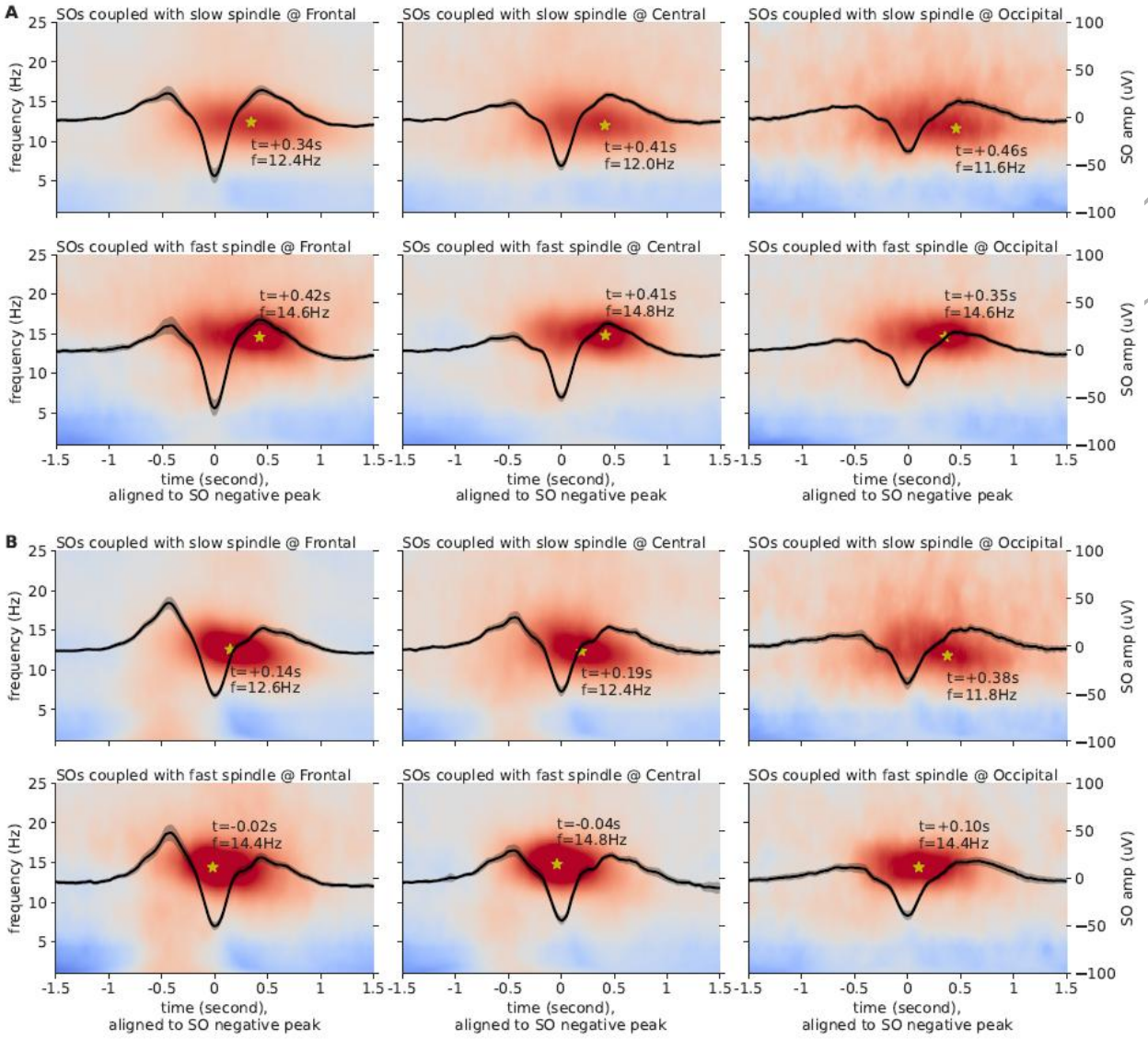

Figure 3. Spindle-SO coupling for the (A) HC and (B) LC. For both panel A and panel B, the two rows represent slow and fast spindle results; the three columns represent frontal, central, and occipital channels. The heatmap displays the EEG spectrogram, time-aligned to the negative peak (trough) of spindle-coupled SOs, and then subtracts the baseline EEG spectrogram, time-aligned to the negative peak of all SOs. The star indicates the location with the highest power in the time-aligned, baseline-subtracted spectrogram, representing the most likely time-frequency of spindles. The black line is the average SO waveform. The shade is the 95% confidence interval of the SO waveform via bootstrapping.

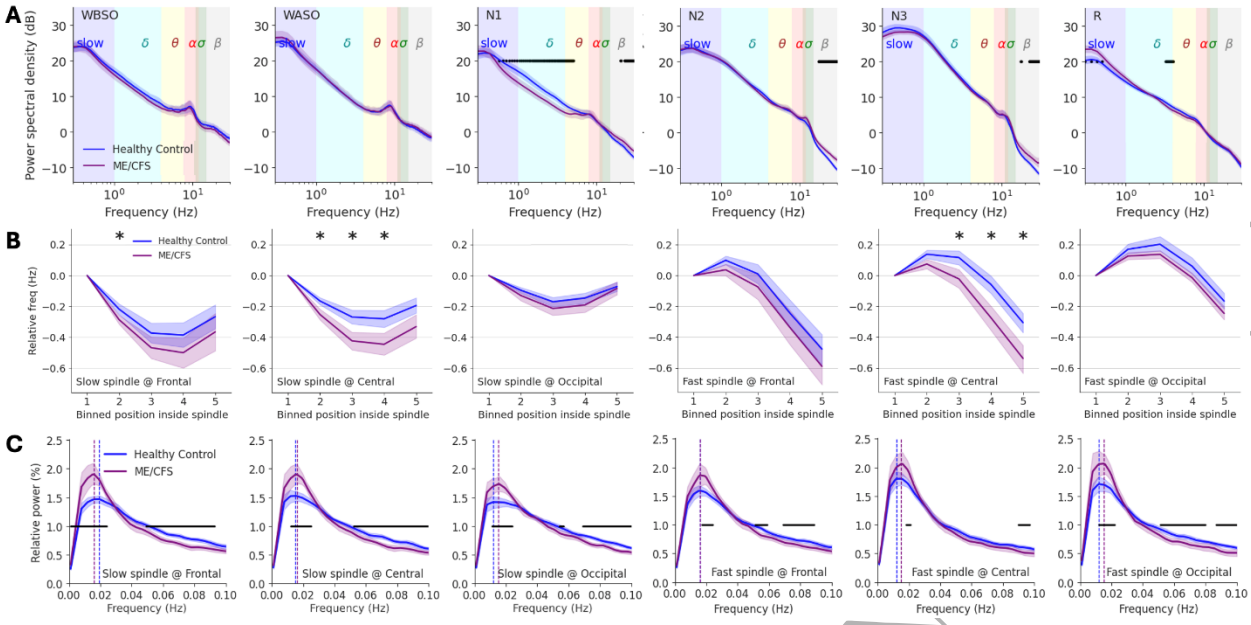

Figure 4. EEG microstructure comparisons between ME/CFS and HC. (A) The spectra of different sleep periods and stages for the HC and ME/CFS groups, averaged between F3-M2 and F4-M1 channels. (B) The instantaneous frequency (IF, frequency within a spindle) over the time course within spindles, partitioned into five bins of equal duration for the HC and ME/CFS groups. The frequencies are relative to the frequency at the first bin to better show the relative change in frequency over time. The purple line represents the ME/CFS group. The blue line represents the control group. The shading represents 95% confidence intervals from bootstrapping 1,000 times. The asterisks represent nonoverlapping confidence intervals (i.e., $p<0.05$). The top row is the fast spindles (≥13Hz). The bottom row is the slow spindles (<13Hz). The left, center, and right columns show the frontal, central, and occipital channels. (C) Infraslow oscillation (ISO) represented by the power spectral density (PSD) of the sigma band power time-series for the healthy controls and ME/CFS group. The ISO peak is around and slightly lower than 0.02Hz. The purple line represents the ME/CFS group. The blue line represents the control group. The horizontal bars represent frequencies that are significantly different based on the bootstrapped confidence intervals. The top row represents ISO PSD derived from slow spindles (<13Hz). The bottom row represents ISO PSD derived from fast spindles (≥13Hz). The three columns represent frontal, central, and occipital channels.

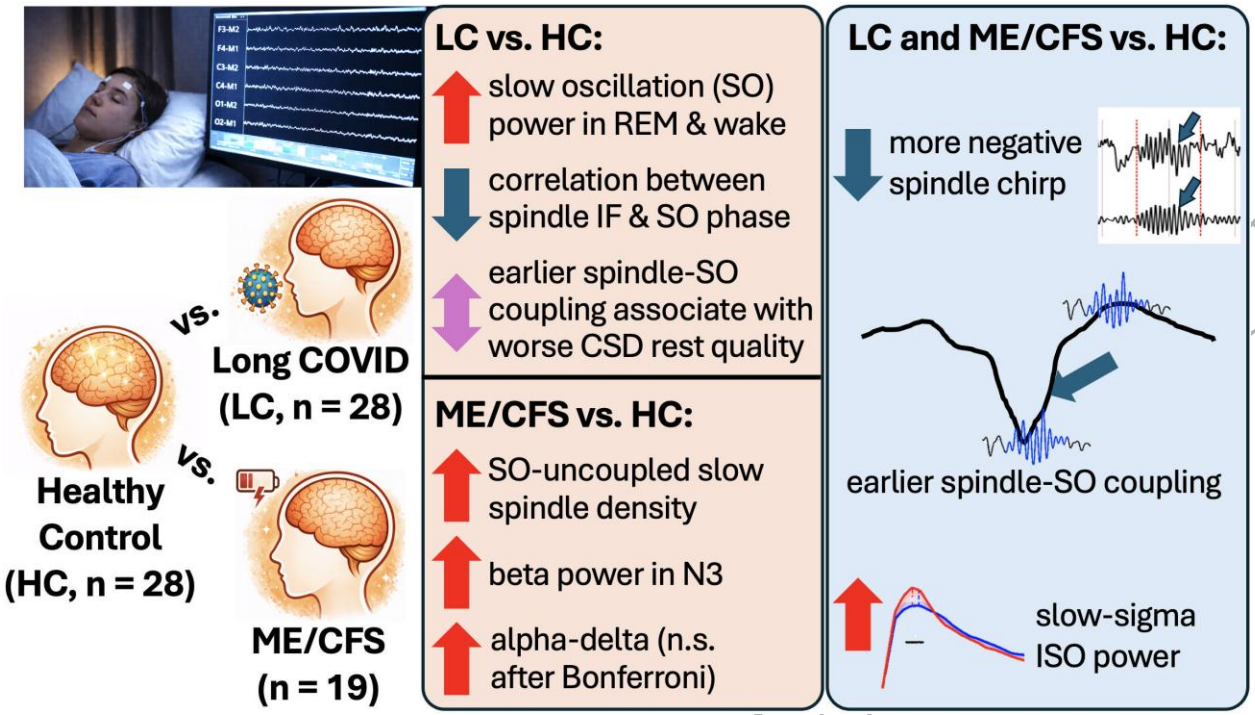

Graphical abstract

TABLES

Table 1. Cohort characteristics for participants in healthy control, long COVID, and ME/CFS groups.

	Healthy Control (n = 28)	**Long COVID (n = 28)** [+]	**ME/CFS (n = 19)** [+]
Age (year): mean ± SD[&]	37.0 ± 11.5	38.2 ± 10.7	40.9 ± 12.5
Sex: n of female (%female)	20 (71.4%)	20 (71.4%)	14 (73.7%)
Race: n (%) (Others are not shown)		*	*
Asian	2 (7.1%)	0 (0.0%)	0 (0.0%)
Black	10 (35.7%)	0 (0.0%)	0 (0.0%)
White	16 (57.1%)	24 (85.7%)	17 (89.5%)
Body mass index (BMI) (kg/m^2): mean ± SD	26.2 ± 4.4	27.8 ± 6.3	24.7 ± 5.7
Sleep parameters: median (interquartile range)			
Apnea-hypopnea index (AHI) (/hour)[^]	1.1 (0.7-2.7)	0.5 (0.3-1.9)	1.5 (0.6-2.2)
Total sleep time (hour)	7.3 (7.1-7.5)	6.7 (5.8-7.3)**	6.0 (5.5-6.7)***
Sleep efficiency (%)	91.8 (89.7-94.1)	83.6 (74.6-90.8)***	87.2 (73.6-89.5)***
Wake after sleep onset (WASO) (minute)	28.8 (15.2-37.5)	27.5 (19.6-59.6)	38.0 (29.8-76.5)**
Sleep latency (minute)	6.5 (3.2-15.2)	17.8 (4.9-49.4)*	22.0 (9.2-28.8)*
REM latency (minute)	88.2 (69.4-127.2)	143.5 (91.2-209.2)*	169.8 (148.0-218.0)***
REM time (minute)	99.8 (81.6-115.5)	83.5 (43.1-95.1)*	53.5 (41.5-70.0)***
N1 time (minute)	29.0 (20.8-45.2)	33.2 (24.1-42.4)	38.5 (28.8-62.5)
N2 time (minute)	223.2 (202.8-251.1)	199.0 (171.9-223.8)*	192.0 (167.5-217.0)*
N3 time (minute)	81.2 (39.2-98.9)	74.5 (56.5-102.1)	70.0 (32.2-100.8)
REM percent (%)	20.4 (18.2-24.6)	16.2 (8.6-18.8)*	12.0 (8.9-15.1)***
N1 percent (%)	5.9 (4.5-8.8)	7.0 (5.4-8.9)	9.0 (6.1-13.4)
N2 percent (%)	46.4 (39.3-53.2)	40.7 (35.3-46.4)*	44.6 (35.3-51.3)
N3 percent (%)	16.6 (8.2-20.6)	17.9 (10.9-21.1)	15.1 (6.8-23.8)
REM continuation probability (%)[$]	95.3 (92.5-96.1)	94.9 (92.5-95.9)	96.5 (95.3-97.0)*
N1 continuation probability (%)	49.0 (43.6-53.2)	59.6 (47.4-66.8)*	61.3 (54.7-72.5)***
N2 continuation probability (%)	89.6 (87.3-93.5)	88.9 (87.1-91.8)	92.0 (84.9-93.7)
N3 continuation probability (%)	93.5 (86.9-95.8)	90.3 (89.1-92.4)	89.8 (58.6-92.9)*
W continuation probability (%)	77.0 (66.0-84.7)	87.3 (81.0-91.5)*	88.4 (72.0-89.8)*
N1 bout duration (minute)[#]	3.2 (2.0-4.0)	4.0 (2.6-6.6)	5.0 (3.8-9.0)***
N2 bout duration (minute)	28.5 (22.5-36.5)	24.8 (21.1-28.2)	25.5 (19.8-33.0)
N3 bout duration (minute)	31.5 (20.8-43.5)	27.2 (18.1-34.8)	29.0 (5.0-38.8)
REM bout duration (minute)	23.0 (18.4-34.6)	21.2 (14.9-28.2)	25.5 (20.8-38.8)
REM time in first half of the night (minute)	29.5 (23.5-45.9)	16.5 (7.0-41.2)	15.0 (1.8-23.5)***
REM percent in first half of the night (%)	13.6 (9.8-19.4)	7.3 (5.1-17.4)	6.3 (0.8-10.5)***
REM time in second half of the night (minute)	68.2 (50.9-81.0)	47.2 (31.2-74.9)*	38.5 (28.0-53.0)***
REM percent in second half of the night (%)	29.4 (21.7-34.1)	20.7 (15.8-30.9)	17.6 (14.0-22.6)***
Subject sleep quality			
CSD Rest Quality (1 is worst resting, 5 is best resting): median (interquartile range)	N.A.	2.4 (1.9-2.9)	N.A.

PROMIS-SD (binary): n (%)	N.A.	8 (28.6%) high sleep disturbance	N.A.

[&] SD = standard deviation. [+] compared to healthy control, * means $p < 0.05$; ** means $p < 0.01$; *** means $p < 0.001$. For age and BMI, the statistical test was t-test. For sex, the statistical test was Fisher's exact test. For race, the statistical test was chi-squared test. For all sleep parameters, the statistical test was Mann-Whitney U test since they do not necessarily follow normal distribution. [^] Hypopnea was scored at 3% desaturation rule. [$] Stage continuation probability is defined as the proportion of having the same stage in the next 30-second epoch across the night from lights off to lights on. [#] Stage bout duration is defined as the maximum duration of continuously being in one stage across the night from lights off to lights on. N.A. = Not Available.

Table 2. Sleep EEG microstructures that were significantly different between healthy controls (HCs) and the long COVID (LC) group, or between HCs and ME/CFS. They are grouped by categories after adjusting for BMI. The p-values are presented after the Bonferroni correction. Rows with a non-empty value in the "LC Median" column indicate sleep EEG microstructures that differ between LC and HC; rows with a non-empty value in the "ME/CFS Median" column indicate sleep EEG microstructures that differ between ME/CFS and HC. We shaded the rows with values in both "LC Median" and "ME/CFS Median" columns, representing the sleep EEG microstructures with shared differences compared to HC between LC and ME/CFS.

Category	**Sleep EEG Microstructure**	**HC Median**	**LC Median**	**ME/CFS Median**
Band power	Slow oscillation power (0.5-1Hz) at REM, frontal (dB)	17.7	20.6**	
	Slow oscillation power (0.5-1Hz) at WBSO, frontal (dB)	21.4	25.0**	
	Beta power (12-30Hz) at N3, occipital (dB)	6.2		9.5*
Fast spindle (≥13Hz)	Fast spindle chirp, central (Hz/second)	-0.20	-0.32**	-0.28*
	Correlation between fast spindle IF[^] & SO phase, central	0.51	0.36**	
	Correlation between fast spindle IF[^] & SO phase, frontal	0.45	0.27*	
	Fast spindle-SO coupling phase, central (degree)	278.0	79.3**	73.2**
	Fast spindle-SO coupling phase, frontal (degree)	212.9	89.3**	83.4**
	Fast spindle-SO coupling phase, occipital (degree)	210.2	90.4**	72.5**
Slow spindle (<13Hz)	Slow spindle density, central (/minute)	1.3		1.8**
	SO-uncoupled slow spindle density, central (/minute)	1.1		1.7**
	SO-uncoupled slow spindle density, frontal (/minute)	1.7		2.3**
	Slow spindle integrated activity, central	0.7		0.8*
	Slow spindle-SO coupling phase, central (degree)	217.0	105.1**	91.3**
	Slow spindle-SO coupling phase, frontal (degree)	247.8	108.0**	90.6**
Slow oscillation (SO, 0.5-1Hz) in NREM	SO positive peak duration, frontal (second)	0.50	0.45**	
	SO rising slope, central (uV/second)	264.3	326.3*	
Infraslow oscillation (ISO, 0.005-0.03Hz) in NREM	ISO relative power from slow sigma, central (%)	36.7		41.3**
	ISO relative power from slow sigma, frontal (%)	35.1	38.3*	40.8**
	ISO relative power from slow sigma, occipital (%)	35.9		38.6**
	ISO relative power from fast sigma, occipital (%)	39.3		44.3*

[*] $p < 0.01$ compared to HC, [**] $p < 0.001$ compared to HC. [^] IF: instantaneous frequency.

Table 3. The correlations between subjective sleep quality and sleep EEG microstructure and macrostructure. The results were obtained from the LC cohort with a sample size of 28, after adjusting for age and sex. Only results with $p<0.05$ are shown.

Category	Sleep Metric	Brain Region	Spearman's Correlation [95% CI]
CSD Rest Quality (the higher the better sleep quality)			
Macrostructure	N2 continuation probability	--	0.54 [0.19, 0.77]
Spectral power	Theta power (4-8Hz) at N2/N3	Frontal	-0.42 [-0.70, -0.04]
Spindle-SO coupling	Fast spindle-SO coupling phase	Central	0.43 [0.05, 0.70]
	Fast spindle-SO coupling overlap	Occipital	0.40 [0.02, 0.68]
Fast spindle	Min-max range of fast spindle frequency	Central	-0.40 [-0.68, -0.01]
	Min-max range of fast spindle frequency	Occipital	-0.43 [-0.70, -0.05]
	Fast spindle frequency	Occipital	-0.41[-0.69, -0.02]
	SO-coupled fast spindle density	Occipital	0.41 [0.03, 0.69]
Slow spindle	Min-max range of slow spindle frequency	Central	-0.56 [-0.78, -0.22]
SO	SO density	Occipital	0.48 [0.12, 0.73]
PROMIS-SD (the higher the worse sleep quality)			
Macrostructure	N1 continuation probability	--	-0.45 [-0.71, -0.08]
Slow spindle	Min-max range of slow spindle frequency	Central	0.43 [0.05, 0.70]
	SO phase correlation with slow spindle frequency	Central	0.47 [0.10, 0.72]
SO	SO positive slope	Central	0.40 [0.01, 0.68]
	SO density	Occipital	-0.42 [-0.69, -0.03]